Drought sensitivity of patterned vegetation determined by rainfall-land surface feedbacks

Alexandra G. Konings,[1] Stefan C. Dekker,[2] Max Rietkerk,[2] and Gabriel G. Katul[1,3]

Received 23 April 2011; revised 15 July 2011; accepted 18 July 2011; published 21 October 2011.

[1] Vegetation pattern morphology is suggested as one indicator of system closeness to desertification. Using pattern morphology as an indicator requires understanding the timescales at which patterned vegetation systems respond to drought. Modeling these timescales requires accounting for rainfall intermittency and all the pathways controlling vegetation-precipitation feedbacks. In this paper, a model of rainfall initiation and intensity based on the dynamics of a single-column atmospheric boundary layer is coupled to a patterned vegetation model. The coupled climate-vegetation model, parameterized to represent a typical vegetation morphology in southwestern Niger, is used to investigate the timescales of desertification due to shifts in the total annual rainfall regime, and the effect of precipitation feedbacks on these timescales. Depending on the exact rainfall history, biomass and spatial morphology may not respond monotonically to a decrease in rainfall. The model results suggest changes in pattern morphology responding to shifts in annual rainfall require at least 4–5 years. Feedbacks acting through vegetation's influence on surface albedo and, to a lesser extent, surface evapotranspiration act to speed up the vegetation response to drought. Although the overall local-scale vegetation-precipitation feedback is positive, individual storm events may exhibit negative feedbacks, in which rainfall only occurs for low vegetation cover, depending on the free atmospheric conditions. Vegetation-precipitation feedbacks are sufficiently important to speed up changes in vegetation patterns, even in marginal drylands with low biomass levels.

Citation: Konings, A. G., S. C. Dekker, M. Rietkerk, and G. G. Katul (2011), Drought sensitivity of patterned vegetation determined by rainfall-land surface feedbacks, *J. Geophys. Res.*, *116*, G04008, doi:10.1029/2011JG001748.

1. Introduction

[2] In many arid and semi-arid regions, vegetation patches form spatial patterns such as spots or labyrinthine stripes. Such patches have been modeled using an activator-inhibitor or Turing-type model, wherein enhanced infiltration capacity beneath vegetated sites and/or extensive lateral root networks promote patch growth at small scale, but inhibit it at larger scale because of competition for water [*HilleRisLambers et al.*, 2001; *Barbier et al.*, 2006]. The models indicate that pattern type depends on the average annual rainfall rates [*Rietkerk et al.*, 2002], and that significant hysteresis exists in these systems [*van de Koppel et al.*, 2002; *Rietkerk et al.*, 2004]. These factors have sparked significant interest in using pattern morphology as indicators of desertification, capable of identifying systems that are close to an "irreversible" shift in vegetation cover toward bare soil. While the role of average annual rainfall rates on steady state vegetation development has been studied repeatedly, two interrelated issues have not yet been fully addressed: the effect of variable rainfall dynamics and concomitant transient behavior in biomass and vegetation morphology, and the existence of feedbacks between the land surface and rainfall in patterned vegetation systems. In this paper, these two issues are studied in the context of vegetation patterns occurring in southwestern Niger, where both spotted patterns have been observed [*Barbier et al.*, 2006] and are expected to be common [*Deblauwe et al.*, 2008]. The vegetation patterns studied are assumed to be spotted patterns on flat ground. For such patterns and sites, soil erosion caused by either fluvialor aeolian processes is assumed to have only a negligible effect on pattern morphology dynamics in this study, although they may be as important as rainfall feedbacks on sloped grounds or for other types of patterns [*Saco et al.*, 2007; *Ravi et al.*, 2007, 2010].

[3] With regards to the first issue, little is known about the timescales of vegetation response to shifts in rainfall regimes such as those that might be associated with climatic variability. Over scales larger than those of the patterned vegetation distribution, several studies have found that the greening of Normalized Difference Vegetation Index (NDVI) measurements over the Sahel since the drought ending in the

[1]Nicholas School of the Environment, Duke University, Durham, North Carolina, USA.
[2]Department of Environmental Sciences, Copernicus Institute, Utrecht University, Utrecht, Netherlands.
[3]Department of Civil and Environmental Engineering, Duke University, Durham, North Carolina, USA.

0148-0227/11/2011JG001748

Table 1. Treatment of Precipitation Feedbacks and Dynamics in Some Patterned Vegetation Studies

Study	Precipitation Feedbacks	Precipitation Dynamics
HilleRisLambers et al. [2001]	None	None
Rietkerk et al. [2002] and *van de Koppel et al.* [2002]	None	None
Kefi et al. [2008] and *Thompson et al.* [2008]	None	None
Scheffer et al. [2005]	Parameterized relationship	None
Dekker et al. [2007]	ET feedback	None
Baudena et al. [2008]	ET and radiative feedbacks	None
Janssen et al. [2008]	Monsoon strength feedback, dependent on radiative feedback	None
Guttal and Jayaprakash [2007] and *Ursino and Contarini* [2006]	None	Wet and dry seasons
Baudena and Provenzale [2008] and *Kletter et al.* [2009]	None	Intermittency

mid-1980s can be partially, though not completely correlated to rainfall on timescales of <1 year [*Hermann et al.*, 2005; *Ollson et al.*, 2005]. However, few records exist of the timescales at which vegetation, and particularly patterned vegetation responds to decreases in rainfall due to drought. *Barbier et al.* [2006] noted that fully vegetated cover under both grazing and water stress changed to spotted vegetation patterns over the course of several decades. *Deblauwe et al.* [2011] also observed changes in pattern types in Sudan between remote sensing observations 20 years apart and spanning a drought. The dynamics of the change in pattern, including the fractional time span within the 20 years over which the pattern change occurred, are not known. In the absence of additional field data, one can nevertheless explore the drought sensitivity of patterned vegetation via model runs. What is the model-predicted "inertia" of the vegetation pattern? That is, how do drought timing and duration influence the size and speed of vegetation pattern response? Is it appropriate to compare steady state model results to observed patterns without taking into account the history of how those patterns evolved?

[4] Answering such questions is further complicated by the possibility that the vegetation cover itself affects the amount of rainfall. Depending on atmospheric conditions, higher evapotranspiration (ET) associated with wetter soils may wet the atmosphere sufficiently to enhance rainfall (a positive feedback). Alternatively, under some conditions, increased turbulent mixing in the atmospheric boundary layer associated with higher sensible heat fluxes from dry soils may cause the initiation of convective rainfall (a negative feedback). A sensitivity analysis using global circulation models (GCM) showed that soil moisture-precipitation feedbacks are most common in areas that are neither very wet (when evapotranspiration is sufficiently high to generate rainfall independent of soil moisture), nor very dry (when the atmosphere is too dry to generate rainfall under any conditions) [*Koster et al.*, 2004]. Based on a number of GCM runs, feedbacks are therefore expected to exist in the Sahel [*Koster et al.*, 2006]. However, there is still some disagreement about the sign of these feedbacks [*Taylor and Ellis*, 2006; *van den Hurk and van Meijgaard*, 2010]. Because the strength of these feedbacks depends on the soil moisture and surface energy partitioning, changes in vegetation cover can also be associated with changes in rainfall. Vegetation can induce precipitation feedbacks by changing the surface energy balance in two main ways [e.g., *Dekker et al.*, 2010]: (1) by changing the surface albedo and therefore the net radiation and (2) by changing the latent and sensible heat fluxes to the atmosphere resulting from a given amount of available radiation and soil water. The feedbacks operating through each of these pathways are referred to here as the "radiative feedback" and "evapotranspiration feedback," respectively.

[5] Only a handful of studies have considered vegetation patterns in the context of dynamic rainfall and these two vegetation-precipitation feedbacks. As shown in Table 1, most studies did not include either vegetation-precipitation feedbacks or precipitation dynamics, and no studies have included both. Table 1 is not meant to be an exhaustive listing of all patterned vegetation studies, but a sample of how precipitation-vegetation patterning is currently being treated.

[6] Several studies have considered the role the vegetation-infiltration relationship supporting patterning plays in determining the size of the vegetation-precipitation relationship [*Scheffer et al.*, 2005; *Dekker et al.*, 2007; *Baudena et al.*, 2008; *Janssen et al.*, 2008]. *Dekker et al.* [2007] used a linear relationship between precipitation amount and evapotranspiration to show that local feedbacks between biomass and soil moisture may cause large-scale vegetation-precipitation feedbacks to be underestimated by as much as 35%. Since far smaller shifts in steady state rainfall can cause changes in spatial vegetation pattern morphology [e.g., *Rietkerk et al.*, 2002; *Thompson et al.*, 2008], such a large feedback implies coupled vegetation-rainfall models are necessary before informed ecosystem management decisions can be made purely from spatial vegetation patterns. *Janssen et al.* [2008] performed a similar study in the context of precipitation feedbacks occurring through large-scale monsoon strength variation.

[7] Vegetation-precipitation feedbacks depend on a large number of interacting processes that create a highly nonlinear relationship between the land surface and the boundary layer structure, which controls the predisposition to precipitation occurrence [*Ek and Holtslag*, 2004; *Santanello et al.*, 2007; *van Heerwaarden et al.*, 2009]. As a result, land surface-precipitation feedbacks are only possible under a limited range of free atmospheric conditions [*Konings et al.*, 2010]. These conditions are limited further by the seasonal nature of the hydrologic cycle in the Sahel, which essentially terminates the feedback mechanisms at the start of the dry season. Earlier estimates of the influence of precipitation feedbacks on patterned vegetation may therefore have overestimated the size of the vegetation-precipitation feedback. Consideration of the non-linearities associated with coupled land surface-atmospheric processes, as well as seasonality, is therefore a logical extension of previous studies.

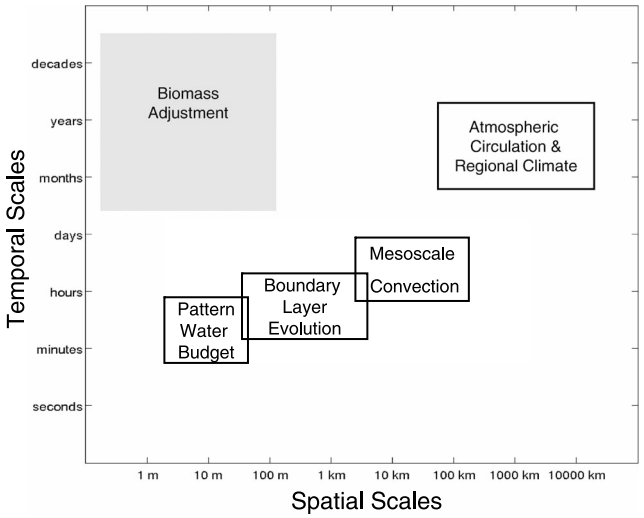

Figure 1. Spatial and temporal scales of the processes impacting vegetation patterns and rainfall occurrence. The temporal scales of biomass adjustment are unknown and are investigated. The pattern water budget is represented by equations (7) and (8); it is coupled to and occurs at roughly the same scales as the surface energy budget. The boundary layer is represented by equations (1)–(3), mesoscale convection is represented by equation (6), and biomass adjustment is dependent on equation (14). Atmospheric circulation and regional climate are represented by the parameters of equations (1) and (2).

[8] In this paper, a one-dimensional atmospheric boundary layer (ABL) model is coupled to a patterned vegetation model to explore the sign and size of vegetation-precipitation feedbacks under temporally variable forcing parameters. The coupled model is used to address two questions: (1) How and how fast do modeled vegetation patterns respond to changes in rainfall regime? (2) How do vegetation-precipitation feedbacks, both those acting through changes in the radiative balance and those acting through changes in evapotranspiration, affect this response? To address these questions, a stationary state for the coupled model is perturbed with changes in rainfall depth of different sizes to simulate initiation of a drought. The response of both vegetation and dynamic precipitation is then analyzed in the context of questions 1 and 2.

2. Methods

2.1. Conceptual Framework

[9] Coupling vegetation-infiltration feedbacks in patterned systems to precipitation variability is difficult due to the large differences in relevant scales between the two processes. Explicitly resolving all relevant scales is computationally infeasible. Instead, a minimalist model that captures certain processes without explicitly resolving them is proposed. As a starting point for building such a minimalist model, Figure 1 illustrates the temporal and spatial scales associated with the key processes that influence vegetation and rainfall fields. Overland water transport between bare soil and vegetated patches allows the increased infiltration over vegetated sites that permits patches to persist, a transport process that requires seconds to minutes. A minimalist model of rainfall at a given site requires resolving the development of the ABL over the course of the day. The intersection of the evolving ABL with the level of free convection is a necessary, though not sufficient, condition for rainfall to occur [*Findell and Eltahir*, 2003]. Once initiated, clouds over an area of tens to hundreds of kilometers may develop into a mesoscale convective system. Their growth and spatial movement is determined by land surface conditions over the extent and duration of the system. Seasonal variability determined by regional climate affects the ability of the turbulent boundary layer to grow to a height promoting rainfall occurrence. In the Sahel, climate is dominated by a single monsoon season lasting roughly from April to October. This climatic variability can be included in a one-dimensional atmospheric boundary layer model by appropriately varying the forcing parameters that modulate lateral heat and moisture transport and entrainment of warm, dry air at the top of the ABL. Such parameters can be estimated from radiosonde measurements, obviating the need for detailed climatic simulations. However, these parameters are controlled by regional climate and atmospheric circulation on scales of hundreds to thousands of kilometers.

[10] In this study, only local-scale vegetation-precipitation feedbacks are considered. The model used here cannot account for feedbacks due to changes in monsoon strength, such as those studied by *Janssen et al.* [2008]. The sensitivity of the monsoon strength to vegetation cover morphology operates over far larger spatial scales than those considered here. At the spatial scales of tens and hundreds of kilometers that are relevant to the monsoon strength, much variability in vegetation morphology is expected. Indeed, vegetation patterns are unlikely to cover the entire zone of influence (see, for example, the variability in the map of predicted pattern occurrence of *Deblauwe et al.* [2008]). To account for local-scale feedbacks, a one-dimensional ABL model driven by large-scale forcing parameters determined from sounding observations is coupled to a vegetation pattern model. The vegetation pattern model of *Kefi et al.* [2008] is revised to include a radiative and an energy balance that allows prediction of the diurnal evolution of average surface sensible and latent heat fluxes, a necessary driver for the ABL and therefore the rainfall model.

2.2. ABL Model

[11] The surface sensible and latent heat fluxes determined by the revised vegetation pattern model are used to drive the dynamics of the atmospheric boundary layer, which is used in turn to predict rainfall occurrence. Large eddy simulation studies have shown that land surface heterogeneity must be on the order of several kilometers in wavelength before the boundary layer development is affected [*Avissar and Schmidt*, 1997]. Since the heterogeneity associated with vegetation patterns occurs on scales several orders of magnitude smaller (see Figure 1), it is not necessary for the boundary layer to be modeled in three dimensions. The ABL model used is equivalent to the model by *Konings et al.* [2010] and is included here for completeness. A so-called slab model is used for the convective ABL, determining average values for potential temperature and specific humidity in the boundary layer and the boundary layer height h throughout the day. The boundary layer is thus assumed to be sufficiently well-mixed

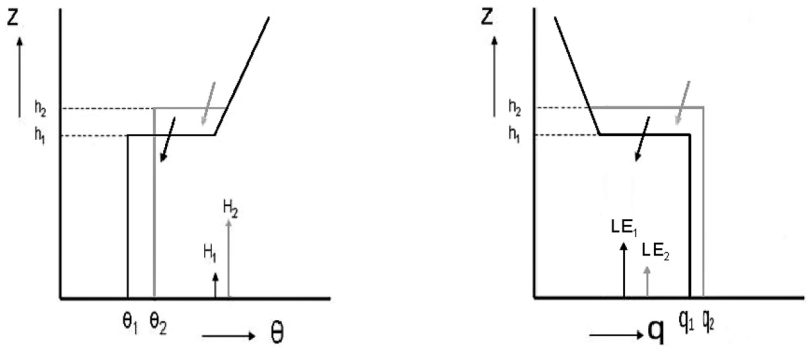

Figure 2. Conceptual model of boundary layer structure at a time t_1 (black line) and a time t_2 (gray line) later in the day. (left) Profile of potential temperature θ_1 is constant with height until the boundary layer height h_1, where an infinitesimally thin inversion occurs. Above h_1, θ increases linearly with height (equation (1)). At the surface, a sensible heat flux H_1 into the boundary layer exists (upward arrows). At h_1, a flux of heat into the boundary layer occurs due to the entrainment of warm air (downward arrows). These fluxes act to change the boundary layer to θ_2 and h_2 over time, as represented by the gray lines. Because h is higher at t_2, entrained air is warmer. (right) The profile of the boundary layer humidity q_1. q_1 is constant with height until the inversion at h_1. Above h_1, q_1 decreases linearly with height (equation (2)). Opposing humidity fluxes exist at the surface (latent heat flux due to evaporation LE, upward arrows) and at h_1 (entrainment of dry air, downward arrows). When the entrainment flux at the top of the boundary layer is higher than the latent heat flux at the surface, the boundary layer q decreases with time. The size of the entrainment flux at the top of the boundary layer varies with the difference between q above and below the inversion. When h increases at time t_2 due to the sensible heat fluxes, the entrainment flux at the top of the boundary layer may therefore be lower.

that the potential temperature θ and the specific humidity q are constant. In the free atmosphere above h, both θ and q are assumed to vary linearly with height above the surface z. Thus,

$$\theta(z) = \gamma_\theta z + \phi_\theta \tag{1}$$

$$q(z) = \gamma_q z + \phi_q. \tag{2}$$

The two sets of slope (γ) and intercept (ϕ) parameters are determined by climatic conditions and are further clarified below. Warm, dry air is mixed into the boundary layer from above (through entrainment) at a rate proportional to the temperature and humidity gradients between the free atmosphere right above the boundary layer and the boundary layer itself. The bottom of the ABL is heated and moistened by surface sensible and latent heat fluxes, respectively. Figure 2 illustrates these assumed profiles and the fluxes driving their dynamics.

[12] The growth of the boundary layer height h in time t is determined by [*Garratt*, 1992]

$$\frac{dh}{dt} = \frac{(1+2A)\overline{(\theta'\omega')_s}}{\gamma_\theta h}, \tag{3}$$

where $\overline{(\theta'\omega')_s}$ is the surface sensible heat mass flux determined as part of the surface energy balance, and A is the Tennekes parameter, defined as the ratio of the sensible heat flux at the top of the boundary layer to the surface sensible heat flux. A is assumed to be constant and is taken to equal 0.2 [*Kim and Entekhabi*, 1998]. As vegetation increases the latent heat flux from the surface, less energy is available for sensible heating of the atmosphere, and the boundary layer grows more gradually. The flux of heat and humidity at the top of the growing boundary layer is proportional to the difference between the value right above the top of the ABL (i.e., $\gamma_\theta h + \phi_\theta$ and $\gamma_q h + \phi_q$) and that right below it (i.e., the value of the ABL itself). Conservation equations can be used to determine the dynamics of the ABL temperature and humidity,

$$h\frac{d\theta}{dt} = \overline{(\theta'\omega')_s} + (\gamma_\theta h + \phi_\theta - \theta)\frac{dh}{dt} \tag{4}$$

$$h\frac{dq}{dt} = \overline{(q'\omega')_s} + (\gamma_q h + \phi_q - q)\frac{dh}{dt}, \tag{5}$$

where $\overline{(q'\omega')_s}$ is the surface latent heat mass flux. The $\overline{(q'\omega')_s}$ and $\overline{(\theta'\omega')_s}$ are related to the latent and sensible heat energy fluxes determined in section 2.3 through $\overline{(q'\omega')_s} = LE/\rho\lambda$ and $\overline{(\theta'\omega')_s} = H/\rho c_p$, where ρ and c_p are the density and specific heat of air, respectively.

[13] The effect of subsidence or vertical motion is neglected in the above model of ABL development, as is typical for single-column slab models. Vertical motion may be significant in the Sahel during August of particularly wet years but is not particularly strong during dry years [*Nicholson and Webster*, 2007]. Nevertheless, it may still be important on individual days.

[14] Convective rainfall is only possible when the ABL height crosses the level of free convection (LFC), the height at which lifted surface parcels become buoyant. In the model, rainfall is possible only if the ABL crosses the lifting condensation level (LCL), the height at which condensation starts. To ensure parcels have sufficient buoyancy to rise the distance from the LCL to the LFC, an additional condition that $z/L \geq 5$ is imposed, where L is the Obukhov length $L = u_*^3\theta/\kappa_v g\overline{(\theta'\omega')_s}$ [*Kader and Yaglom*, 1990]. This condition is

evaluated at the center of the boundary layer, $z = h/2$. The κ_v is von Kármán's constant, g is gravitational acceleration, and u_* is the friction velocity. Since no friction velocity measurements are available for patterned vegetation systems in Niger, we use half-hourly eddy-covariance observations (temporally interpolated to the model time step of 2.5 min, which is chosen to ensure stability and accuracy of the ABL model development) ensemble averaged over a variety of sites. The diurnal cycles of all sites are similar, providing confidence that using data from different locations is appropriate for use in this model of rainfall in the Sahel, at least in a first order estimate.

[15] When rainfall occurs, the amount of rainfall is equal to a fraction η of the total water vapor in the atmospheric column. The height over which free atmospheric moisture is non-zero, given by ϕ_q/γ_q, can vary considerably depending on variations in γ_q and ϕ_q. The water column from which precipitation (R) is drawn is therefore capped at $2h$ to prevent unrealistic sensitivity to small fluctuations in the free atmospheric parameters and is given as

$$R = \eta \int_{z=0}^{z=2h} q dz. \tag{6}$$

The η integrates a whole range of processes that determine rainfall efficiency, including the availability of condensation nuclei (i.e., dust and other aerosols), cloud depth, and age. The effects of these combined factors are difficult to model, and they are lumped into a single parameter here.

[16] For simplicity, each rainstorm is assumed to be distributed over two hours. Although this is almost certainly a gross simplification of the actual rainfall description, modeling storm distribution is beyond the scope of this simple model. A further simplification is that the effect of cloud cover is not explicitly accounted for. Since storm dynamics are not explicitly represented, the additional effect of not representing cloud cover explicitly on days when rain occurs is likely to be low. The effect of cloud cover on days without rain is discussed below. Nevertheless, by having rainfall occurrence and amount depend on vegetation and climatic conditions via surface and free atmospheric fluxes, respectively, the model captures many of the processes and timescales that determine vegetation-precipitation feedback occurrence. At night, the ABL collapses and becomes stable. It is assumed that no rainfall occurs at night, another idealization of reality.

2.3. Surface Cover Model

[17] The vegetation pattern model used here is revised from *Kefi et al.* [2008] to include an energy balance and to account for drought-adaptation mechanisms. It consists of three state variables, the biomass P, the subsurface water content W, and the surface water content O. The dynamics of surface water are modeled according to

$$\frac{\partial O}{\partial t} = R - \alpha_0 \frac{P + k_2 W_0}{P + k_2} O + D_O \nabla^2 O, \tag{7}$$

where O is increased by precipitation of rate R and continually loses water to infiltration at a rate $\alpha_0[(P + k_2 W_0)/(P + k_2)]$. The α_0 is the maximum infiltration rate, k_2 is the saturation constant of infiltration, and W_0 is the relative infiltration rate over bare soil. The infiltration rate is taken proportional to the amount of surface water O. Overland flow of water is modeled as a diffusive process with diffusivity D_0. Although this is a poor approximation of the physical processes governing surface flow, the flow is assumed sufficiently fast relative to other processes that the exact routing mechanism of water from the soil to the vegetation does not impact the total amount of infiltrated water in vegetation patches and therefore does not influence the patch growth.

[18] The evolution of subsurface water is modeled as

$$\frac{\partial W}{\partial t} = \alpha_0 \frac{P + k_2 W_0}{P + k_2} O - E_t - E_s - r_w W + D_W \nabla^2 W, \tag{8}$$

where W is gained from infiltration, but lost due to transpiration at a rate E_t, soil evaporation at a rate E_s, and deep soil drainage at a rate $r_w W$. Lateral transport is once again modeled as a diffusive process, where D_W is the diffusivity of sub-surface water. The E_t and E_s are modeled by calculating the latent heat of transpiration LE^t and soil evaporation LE^s. The Penman-Monteith equation is used in each case, but uses different descriptions of the surface conductance for transpiration and evaporation, respectively. The canonical form of the Penman-Monteith equation is

$$LE = \frac{\Delta(R_n - G) + \dfrac{\rho c_p \mathrm{VPD}}{r_a}}{\Delta + \gamma\left(1 + \dfrac{r_s}{r_a}\right)}, \tag{9}$$

where R_n is the net radiation at the surface, G is the ground heat flux, ρ and c_p are the density and specific heat capacity of air, respectively, and VPD is the vapor pressure deficit. Δ is the slope of the Clausius-Clapeyron equation relating the saturated vapor pressure of water to temperature, and γ is the psychrometric constant, $\gamma = c_p P_s/0.622\lambda$, where P_s is the surface pressure and λ is the latent heat of evaporation of water. The r_a is the aerodynamic resistance, while r_s is the surface resistance, the inverse of the surface conductance g_s. When calculating the transpiration, the surface conductance is the stomatal conductance g_s^{Et}, $r_s = r_s^{Et} = 1/g_s^{Et}$. When using equation (9) to calculate the soil evaporation energy flux LE^s the surface conductance is the conductance over bare soil g_s^{Es}, such that $r_s = r_s^{Es} = 1/g_s^{Es}$. The radiative calculations necessary for the use of equation (9) are further detailed below. Once the latent heat is determined, its components can be converted to the total height of water evaporated or transpired,

$$E_t = \frac{LE^t}{\lambda \rho_{\mathrm{H_2O}}} \tag{10}$$

$$E_s = \frac{LE^s}{\lambda \rho_{\mathrm{H_2O}}}, \tag{11}$$

where $\rho_{\mathrm{H_2O}}$ is the density of water.

[19] The stomatal conductance g_s^{Et} captures the vegetation response to water stress. It is determined by calculating the leaf conductance as a function of water stress (specifically, W and the vapor pressure deficit VPD) and upscaling it to the canopy level depending on the leaf area index. The leaf

area index is calculated as $\alpha_1 P$, where α_1 is the amount of leaf area per unit biomass. The total stomatal conductance is given by

$$g_s^{E_t} = g_{\max}^{E_t} \frac{W}{W + k_1} (1 - m \log(\mathrm{VPD})) \alpha_1 P. \quad (12)$$

where $g_{\max}^{Et}$ is the maximum stomatal conductance per unit leaf area, k_1 is a saturation constant of water stress, m controls the rate of decrease in conductance with increased vapor pressure deficit VPD (in kPa). The saturation function $W/(W + k_1)$ is commonly used to represent patterned vegetation response to water stress [e.g., *HilleRisLambers et al.*, 2001; *van de Koppel et al.*, 2002; *Rietkerk et al.*, 2002]), while $1 - m$ log(VPD) has been found to be an appropriate description of the rate at which stomata close when atmospheric water demand is high (to prevent excessive water loss) across many species [*Oren et al.*, 1999]. This function has also recently been shown to be consistent with stomatal optimization theories [*Katul et al.*, 2009; *de Boer et al.*, 2011]. The soil surface conductance g_s^{Es} used to estimate E_s is given by

$$g_s^{E_s} = g_{\max}^{E_s} \frac{W}{W + k_1} \left(1 - \frac{P}{P + k_3}\right), \quad (13)$$

where $g_{\max}^{Es}$ is the maximum bare soil conductance and k_3 is the saturation constant for the evaporation reduction function due to shade from biomass. The presence of biomass provides physical cover and shading that reduces bare soil evaporation. Incorporating this effect without an explicit model of biomass morphology is difficult, so a simple saturation term $(1 - [P/(P + k_3)])$ is used here.

[20] Plant growth and movement are modeled as a balance between assimilation and respiration,

$$\frac{\partial P}{\partial t} = (g_{\mathrm{CO}_2} c C_1 \alpha_1 P - \mathrm{Resp}(T_{air}) P) \frac{1}{\tau(W)} + D_P \nabla^2 P, \quad (14)$$

where g_{CO_2} is the stomatal conductance with respect to CO_2, c is the concentration gradient of CO_2 between the atmosphere and the intercellular space of the stomata, and C_1 is a conversion factor between carbon gain and biomass growth. The $\mathrm{Resp}(T_{air})$ is the autotrophic respiration as a function of air temperature T_{air} (in Celsius). The $\tau(W)$ function accounts for drought-adaptation mechanisms within the vegetation [*Guttal and Jayaprakash*, 2007]. Last, D_P is the diffusivity of the biomass spread process. Although representing biomass spread as a purely diffusive process is a simplification, *Thompson et al.* [2008] showed that the energetic modes of the vegetation morphology do not change significantly if a more realistic kernel-based method is used. The properties and closure state of the leaf stomata influence both transpiration and assimilation, such that the stomatal conductance with respect to CO_2 and the stomatal conductance with respect to water are linearly proportional.

$$g_{CO_2} = \nu \frac{E_t}{q - q^*}, \quad (15)$$

where ν is the ratio of the stomatal conductance with respect to CO_2 to the stomatal conductance with respect to water, q is the near-surface (here, boundary layer average) specific humidity, and q^* is the specific humidity at saturation. Respiration rates depend on temperature according to

$$\mathrm{Resp}(T_{air}) = R_b Q_{10}^{\frac{T_{air} - 10}{10}}, \quad (16)$$

where R_b is the base respiration rate per unit biomass and Q_{10} is a temperature sensitivity coefficient. The near-surface air temperature varies over the course of the day. By definition, $T_{air} \approx \theta$ near the surface. The use of $\tau(W)$ prevents vegetation from dying during each dry season by accounting for seasonal reduction in metabolic activity [*Guttal and Jayaprakash*, 2007] given as

$$\frac{1}{\tau(W)} = \frac{1}{4} \frac{W^2 + f k_4}{W^2 + k_4}, \quad (17)$$

where k_4 is a saturation constant with respect to subsurface water and f is the metabolic activity in the complete absence of water. To prevent excessive fluctuations, plant biomass is updated daily, at a much coarser timescale than the ABL and water balance models.

[21] The radiation driving transpiration and evaporation is determined by performing a full energy balance at each point in space. The net radiation $R_n(t)$ is given by

$$R_n(t) = (1 - \alpha) R_s(t) + \epsilon_s \left(\epsilon_a \sigma T_{air}^4 - \sigma T_s^4\right), \quad (18)$$

where α is the surface albedo, $R_s(t)$ is the incoming shortwave radiation, ε_s is the surface emissivity, ϵ_a is the atmospheric emissivity, σ is the Stefan-Boltzmann constant, and T_s is the surface temperature. The terms on the right-hand side of equation (18) describe the net shortwave radiation, the downward longwave radiation and the upward longwave radiation, respectively. The $R_s(t)$ is calculated based on astronomical equations, which are described in the appendix. The surface albedo depends on surface vegetation cover and is lower for more vegetated soils. Bare soils in the Sahel are taken to be lighter than their vegetated counterpart. Therefore, albedo is linearly interpolated between $\alpha = 0.25$ at P = 0 and $\alpha = 0.15$ at P = 25 g m^{-2}. For clear sky conditions, ϵ_a depends on the air temperature and air humidity as described elsewhere [*Brutsaert*, 1975]. Surface temperature is evolved by noting that the surface sensible heat flux H depends on the gradient between surface and air temperatures:

$$H = \frac{\rho c_p}{r_a} (T_{air} - T_s). \quad (19)$$

[22] The atmospheric resistance r_a is modeled as $r_a = (h_{ra}/z_o)/\kappa_v u_*$, where h_{ra} is the surface layer height and z_o is the surface roughness height. The roughness height depends on canopy height h_c, $z_o = 0.1 h_c$. The canopy height is assumed to be proportional to biomass, $h_c = 0.05/3P$. H is determined as the residual of the surface energy balance,

$$H = R_n - \lambda \rho E_t - \lambda \rho E_s - G, \quad (20)$$

G is the ground heat flux and is assumed to equal $0.15 R_n$, λ is the latent heat of vaporization of water; λ and ρ are used to convert the latent heat fluxes from mass rates to energy rates. Equations (18), (19),and (20) form a coupled system for R_n,

Table 2. Parameter Values Used in Surface Cover Model

	Definition	Value	Source
r_w	Drainage parameter	0.08 d^{-1}	Adapted from *Dekker et al.* [2007]
D_W	Diffusivity of subsurface water spread	0.1 m^2 d^{-1}	*Rietkerk et al.* [2002]
g^{Et}_{max}	Maximum stomatal conductance	0.01 m s^{-1}	Fitted
k_1	Half-saturation of plant water uptake	3.3 mm	Fitted
m	Conductance VPD-sensitivity	0.6	*Oren et al.* [1999]
α_1	Max. infiltration rate per unit surface water	0.2 d^{-1}	*Rietkerk et al.* [2002]
g^{Es}_{max}	Maximum surface conductance	0.01 m s^{-1}	Fitted
α_0	Fraction of biomass contributing to LAI	0.01 g^{-1} m^{-2}	Fitted
k_2	Saturation parameter for infiltration	5 g m^{-2}	*Rietkerk et al.* [2002]
W_0	Infiltration scaling for bare soil infiltration	0.2	*Rietkerk et al.* [2002]
D_0	Diffusivity of surface water spread	100 m^2 d^{-1}	*Rietkerk et al.* [2002]
k_3	Half-saturation constant for soil shading	2.5 g m^{-2}	Assumed
ν	Stomatal conductance to CO_2 relative to H_2O	0.0259 mm m^{-2} mol^{-1}	*Larcher* [2003], see also derivation by *Kefi et al.* [2008]
c	CO_2 concentration gradient	152 ppm	0.6 ratio of concentration inside and outside stomata [*Katul et al.*, 2000], 380 ppm atmospheric CO_2
C_1	Biomass produced per CO_2 assimilated	0.0017 g mol^{-1}	*Kefi et al.* [2008]
D_P	Diffusivity of biomass spread	0.01 m^2 d^{-1}	*Rietkerk et al.* [2002]
R_b	Base respiration per unit biomass	0.1 d^{-1}	*Kefi et al.* [2008]
Q_{10}	Respiration temperature sensitivity	1.60	*Larcher* [2003]
f	Drought adjustment in absence of water	0.04	*Guttal and Jayaprakash* [2007]
k_4	Drought adjustment scaling parameter	10 mm	*Guttal and Jayaprakash* [2007]
ϵ_s	Surface emissivity	0.97	*Brutsaert* [2005]
h_{ra}	Surface layer height	25 m	Assumed

H, and T_s. This coupled system and the rest of the surface cover model are all evaluated at the same time step as the ABL model. The values for the vegetation parameters are summarized in Table 2.

2.4. Model Parameterization

[23] The coupled model is parameterized such that the final model contains a stationary state in which the biomass forms spatial patterns at a seasonal rainfall rate near 365 mm/yr, or 1 mm/d on average. This is a typical rainfall rate used in patterned vegetation models [e.g., *Rietkerk et al.*, 2002]. For the vegetation component of the model, this is accomplished by altering the α_0, g^{Et}_{max} and g^{Es}_{max} parameters within a plausible range to achieve the typical patterns reported for the Sahel. Note that α_0 and g^{Et}_{max} are species-dependent, while g^{Es}_{max} is soil-dependent. Other vegetation parameters were derived from the models of *Kefi et al.* [2008] and *Rietkerk et al.* [2002].

[24] To realistically parameterize rainfall and represent rainfall-related feedbacks, free atmospheric parameters (i.e., the slope and intercept of the temperature and humidity profiles) are needed. Approximately 2900 daily radiosonde profiles, distributed over 20 years, were used to determine these parameters. The data used are maintained by the University of Wyoming Department of Atmospheric Sciences. The seasonal cycle of the parameters was determined by averaging over all profiles for each day of year. This seasonal cycle is repeated from year to year. The effect of interannual variability in these parameters due to climatic fluctuations is neglected here. By keeping free atmospheric parameters constant from year to year, possible vegetation-precipitation feedbacks associated with land surface-induced changes in large-scale circulation are neglected [*Charney*, 1975]. Linking this feedback mechanism to patterned vegetation requires assuming patterns of a given time are present over very large scales (see Figure 1). This possibility is neglected here for simplicity. Interannual variability in precipitation amounts over variability over the West African Sahel is driven largely by variability in the intensities and frequencies of storms rather than the length of the wet season [*Grist and Nicholson*, 2001]. Since the length of the wet season depends largely on the seasonal evolution of free atmospheric parameters, this provides further support for using free atmospheric forcings that are repeated every year.

[25] The radiosoundings were taken at the Niamey airport in southwestern Niger, at midday (12:00 LT). The boundary layer height is lower than 1500 m by this time. Thus, linear profiles for θ and q are regressed against height for $z \in [1500, 4000]$. In southwestern Niger, long-term raingauge records indicates about 95% of the rain falls between the first day of May and the first day of October [*Lebel et al.*, 1997]. The seasonal cycle of the free atmospheric parameters, shown in Figure 3, roughly supports this behavior. The $|\gamma_q|$ and ϕ_q are higher during the summer monsoon season, allowing the boundary-layer to cross the LCL (which is inversely related to moisture) more readily, such that precipitation occurs for a greater range of surface fluxes. Although γ_θ is also higher during the wet season than during the dry season (allowing the boundary layer to grow higher for a given amount of sensible heating), its seasonal variability is small and shows strong fluctuations during the wet season. This is consistent with the work of *Konings et al.* [2010] indicating the free atmospheric moisture parameter has a greater influence on rainfall occurrence than the free atmospheric temperature profile.

[26] Although the conditions used to model rainfall events are necessary for the triggering and persistence of storms, they are not sufficient. Condensation nuclei size, updraft velocity, and other factors may still limit the production of rainfall. These limiting factors are generally unrelated to the average ABL state and require modeling (and a concomitant set of parameters) that is too detailed to be included here. Instead, each day of the year (DOY) is assigned a binary parameter Π(DOY) that combines the limiting factors above

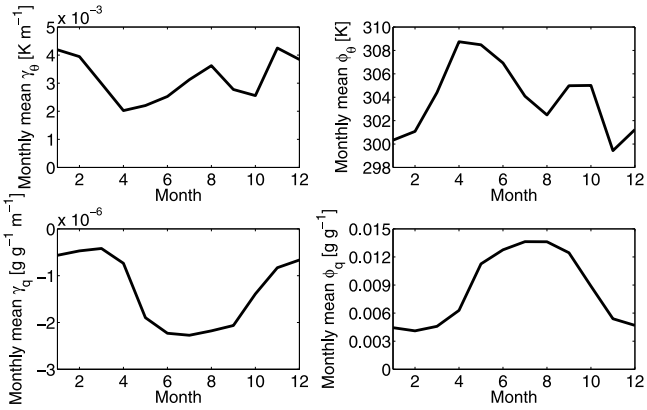

Figure 3. (left) Seasonal cycle of the measured slope γ and (right) intercept ϕ of the linear free atmospheric profiles for (top) potential temperature θ and (bottom) specific humidity q used in equations (1)–(5) as determined from 30 years of radiosonde data collected at Niamey airport, southwestern Niger. For comparison, late afternoon boundary layer heights are generally around 3000 m.

into a single value that either allows or does not allow rainfall to occur. For each day of year, Π(DOY) is determined randomly and independently. The binary distribution from which it is drawn is parameterized such that the total number of storms occurring each year is about 28 (depending on surface conditions), an average value appropriate for southwestern Niger [*Lebel et al.*, 1997]. Moreover, Π(DOY) = 0 during the dry season. Note that although Π(DOY) reflects the strong seasonality of rainfall in Niger, this seasonality is also captured in the free atmospheric parameters. That is, during the dry season, the free atmospheric parameters are such that rainfall is rarely possible under any land surface conditions.

[27] Given Π(DOY), η_{steady} is chosen in equation (6) such that the rainfall intensity of the stationary state is 365 mm/yr (see also section 3 for additional justification for varying η), resulting in $\eta_{steady} = 0.33$. The exact average rainfall for a given location depends, among others, on η (or the average value thereof), which integrates a large range of variables independent of the free atmospheric parameters used (as discussed in section 2.2). Furthermore, vegetation patterns occur throughout much of southwestern Niger [*Deblauwe et al.*, 2008], where spatial variability in rainfall rates is very high. Pattern occurrence in this region is therefore associated with a large range of rainfall rates. Since the free atmospheric parameters used integrate atmospheric conditions on a larger scale than the variability in rainfall, there is no reason to believe the rain rate at the exact location where free atmospheric parameter measurements where made (520 mm/yr at the Niamey airport) is the most appropriate representative value for patterned vegetation systems in the region. Instead, 365 mm/yr is used, as it is a typical rainfall rate used for patterned vegetation studies.

3. Analysis

3.1. Experimental Design

[28] When precipitation is a system variable rather than an externally imposed forcing parameter, systematically controlling the effects of changes in rainfall amount (i.e., drought) is difficult. In the 1-D ABL model above, two factors could be varied to influence the total amount of rainfall: the free atmospheric forcings that determine when and under what conditions rainfall occurs (equations (1)–(5)), and the precipitation efficiency η (equation (6)). The free atmospheric conditions can be altered to model possible changes in large-scale atmospheric circulation that affect rainfall amounts, but doing so would require computationally intensive sampling of the full range of realistic change scenarios for not only each of the four individual parameters, but also their covariances. In contrast, modifying η (in isolation) immediately suggest how total rainfall is likely to change. Because of this tractability, η is used as a control variable throughout. In section 4.1, η is scaled by different amounts to represent droughts of different sizes according to $\eta = \eta_{sc}\eta_{steady}$. For example, when $\eta_{sc} = 0.85$, this is interpreted as a drought with an anomaly size of approximately 15% of the rainfall associated with η_{steady}, which is about 55 mm/yr. Note that due to the presence of vegetation-precipitation feedbacks, this may not be the annual rainfall at any time during the drought. However, η_{sc} provides a framework for defining different drought conditions a priori.

[29] As noted earlier, the vegetation state influences the development of the ABL and the resulting precipitation through two main pathways: modification of the amount of latent heating (ET feedback) and modification of the available radiative energy through the vegetation's influence on albedo (radiative feedback). These two pathways are illustrated by the top and bottom lines of Figure 4. The contributions of the two mechanisms to the total feedback effect are investigated in section 4.2. To determine the effects of the feedbacks, each pathway is artificially removed (in separate simulations) from the coupled system. This removal is achieved by replacing P in the above formulations for evapotranspiration and/or albedo (depending on the pathway being studied) with an effective vegetation cover that does not evolve in time. To allow for convenient interpretation of the sign of the feedbacks, this effective cover is designed to have a biomass less than is common even in the peak of the dry season. Its mean biomass is $\approx$3.8 g m^{-2}. The effective vegetation cover is used only in determining the atmospheric boundary layer development and the possibility of rainfall. As in the fully coupled model, infiltration depends on the dynamic vegetation. Vegetation growth depends on the values of the boundary layer VPD and T determined by the fully coupled model. Removing feedbacks solely in the determination of rainfall ensures consistency and simplifies the comparison of the full and partial vegetation-precipitation feedback cases. In the rest of this paper, the effective vegetation cover is referred to as the vegetation mask.

[30] In a "no radiative feedback" run, dynamic vegetation influences the energy partitioning of the ABL used to determine rainfall, but the shortwave upward radiation and the total available energy are specified according to the "effective" vegetation cover mask. In "no ET feedback" runs, dynamic vegetation influences the total available energy, but the partitioning of that energy into latent and sensible heating is not influenced by the evolution of vegetation, and is instead fixed according to the effective vegetation mask. Section 4.2 applies each of the feedback specifications to the different drought scenarios studied in section 4.1 and

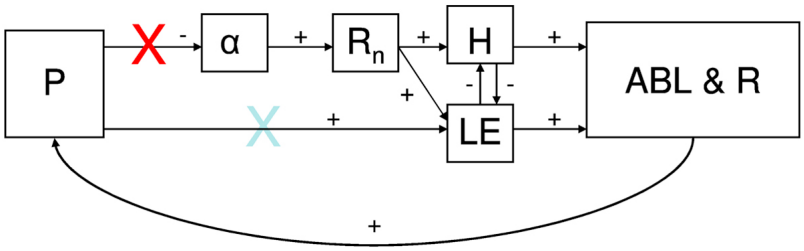

Figure 4. Key pathways of model influence of vegetation biomass on rainfall (R). Biomass influences albedo (α), which influences the surface energy R_n available for latent (LE) and sensible (H) heating. In the "no radiative feedback" simulations of section 4.2, this influence is artificially removed (red cross). Biomass (P) also has a direct influence on the total surface latent heat flux (equations (12) and (13)). In the "no ET feedback" simulations of section 4.2, this influence is artificially removed (blue cross). The dashed line indicates that rainfall also influences biomass.

discusses the effect of each feedback type on the total rainfall and on the resulting vegetation cover for different values of η_{sc}. The relative sizes of the ET feedback and the radiative feedback are also discussed.

[31] For each of the simulations in section 4, the system is initiated with the same end-of-year land surface conditions for the stationary state of the case η_{steady}, representing the "long-term average" rainfall. The η is then scaled by a factor η_{sc} for the entire duration of the 10-yearlong simulation, representing a 10-year drought. For simplicity, interannual variability is ignored throughout, except where it is generated by land surface-precipitation feedbacks.

3.2. Analysis Metrics

[32] To address question 1, it is necessary to track measures of spatial vegetation pattern morphology in time. There is no unique "measure" that captures all aspects of pattern morphology. Instead, all vegetation morphology patterns are characterized by two scalar measures: (1) the mean biomass and (2) the spatial Shannon entropy, representing the pattern type. The Shannon entropy does not depend on the absolute values of biomass, and can therefore be used as an informative scalar measure even when no absolute biomass values are known, such as when data are obtained from remotely sensed images. The two scalar pattern measures used are entirely independent.

[33] The Shannon entropy of a string or field represents the total information content and can be defined as

$$I_u = -\sum_{i=0}^{n} p_i(x)\log(p_i(x)), \tag{21}$$

where n is the number of bins and $p_i(x)$ is the probability that x (here biomass) belongs to bin i. As the system becomes more uniform (and $p_i(x)$ tends to a single value equal to 1/n), the maximum weight log(p) decreases, and the measure goes to zero. To facilitate interpretation, the measure is normalized by I_u for a uniform distribution,

$$I = \frac{\sum_{i=0}^{n} p_i(x)\log(p_i(x))}{-\log(n)}, \tag{22}$$

I now varies between 0 and 1. The normalization also reduces the dependence on the discretization of binning used in the numerical estimation of I. Again, I does not directly depend on the spatial distribution of patterns (that is, two pixels of a given biomass level interspersed with a bare pixel have the same entropy as a cluster of two pixels next to a bare patch.) Nevertheless, the measure can distinguish between different pattern types because different types have different surface area-to-volume ratios. Because biomass is generally reduced at the edges of a patch, the resulting values of $p_i(x)$ differ. This is illustrated in Figures 5a–5d, which shows the different entropies associated with the canonical pattern types, spots, labyrinthine bands, and gaps. Each of the pattern types is simulated using the model of *Rietkerk et al.* [2002]. Although spots and gaps are to some degree "inverse" patterns, their associated entropy is still sufficiently different to be distinguishable. In the case of gaps, the most spatially

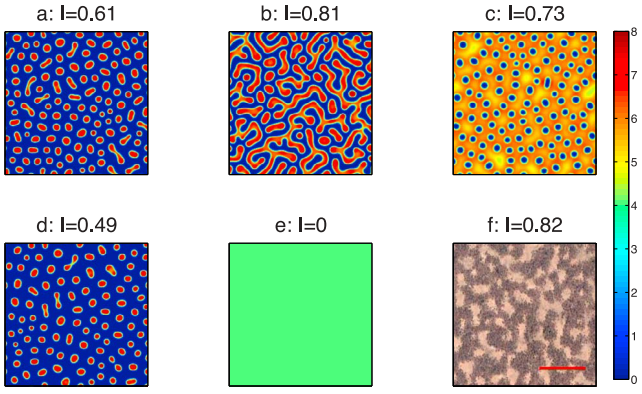

Figure 5. Shannon entropy calculated from biomass images for (a) spotted vegetation patterns, (b) labyrinthine vegetation patterns, (c) gapped vegetation patterns, (d) spotted vegetation patterns, at a lower rainfall rate than those in Figure 5a, (e) a uniform field and (f) an image of vegetation patterns in southwestern Niger. Each of the maps in Figures 5a–5d represent canonical pattern types and are simulated using the model of *Rietkerk et al.* [2002] with a 200 × 200 m grid using rainfall rates R of R = 0.75 mm/d (Figure 5a), R = 1.00 mm/d (Figure 5b), R = 1.25 mm/d (Figure 5c), and 0.65 mm/d (Figure 5d). Figure 5f represents vegetation patterns in southwestern Niger, at 12° 19′54.91N, 3° 10′41.76E. Image taken from Google Earth, copyright 2011 Digital Globe. The red scaling line represents 100 m.

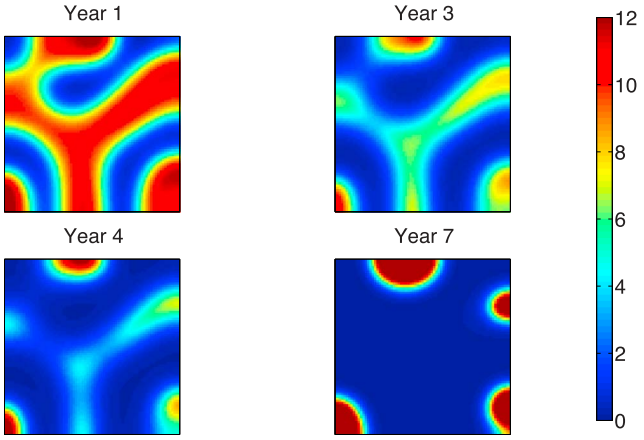

Figure 6. Biomass (g m^{-2}) spatial patterns over a grid of 75 × 75 m for different years after the initiation of a drought with η_{sc} = 0.85. The system evolved from a labyrinthine pattern in year 1 to a spotted pattern in year 7 through the thinning and breaking apart of bands. Remaining vegetation spots then increase in extent.

extensive cover type (i.e., the connected areas of vegetation) still shows some variations in exact biomass level. In the case of spots, the most spatially extensive cover type consists of bare soil with biomass that is essentially zero. The only fluctuations consist of small model imperfections that are too small, relative to the total range of biomass, to affect the information content. As a result, the spatially extensive vegetation in the case of a gapped pattern contributes more to I than the spatially extensive bare soil in the case of spots, and I is distinguishably higher in the case of a gapped pattern than in the case of a spotted pattern. In part f, the observed patterned vegetation in Niger is depicted. It has a I = 0.82, comparable to a labyrinth pattern.

4. Results

4.1. How and How Fast Do Modeled Vegetation Patterns Respond to Changes in Rainfall Regime?

[34] The vegetation changes from a labyrinthine to a spotted pattern as the coupled system responds to drought for the case of η_{sc} = 0.85 (Figure 6). During the transition, bands of vegetation become thinner until they break, leaving individual clusters of vegetation that will eventually make up the spotted pattern. The remaining bands, as well as leftover spots, die out slowly over time. The exact evolution of the system, including the seasonal cycle, can be seen in Animation S1 in the auxiliary material.[1]

[35] The time series of biomass entropy, mean (spatial) biomass, and annual rainfall amount and number of events for droughts of different sizes are shown in Figure 7. The η_{sc} = 1 corresponds to $\eta = \eta_{steady}$ and represents the long-term steady state conditions before the start of the drought. Although the rainfall decreases in all cases, biomass slightly increases when η_{sc} = 0.95; this is further discussed in section 4.2. The timescale of vegetation adjustment to changes in rainfall depends on the size of the drought. While vegetation amount and spatial pattern adapt to the small reduction in rainfall resulting from η_{sc} = 0.95 (about 17 mm/yr) on timescales <1 year, it takes about 4 years for the vegetation to die out completely when η_{sc} = 0.8.

[36] When η_{sc} = 0.85, both the patterns and the mean biomass require more than 10 years to adapt to a new steady vegetation pattern. For the first 6 years of the drought, vegetation biomass steadily decreases, and the vegetation

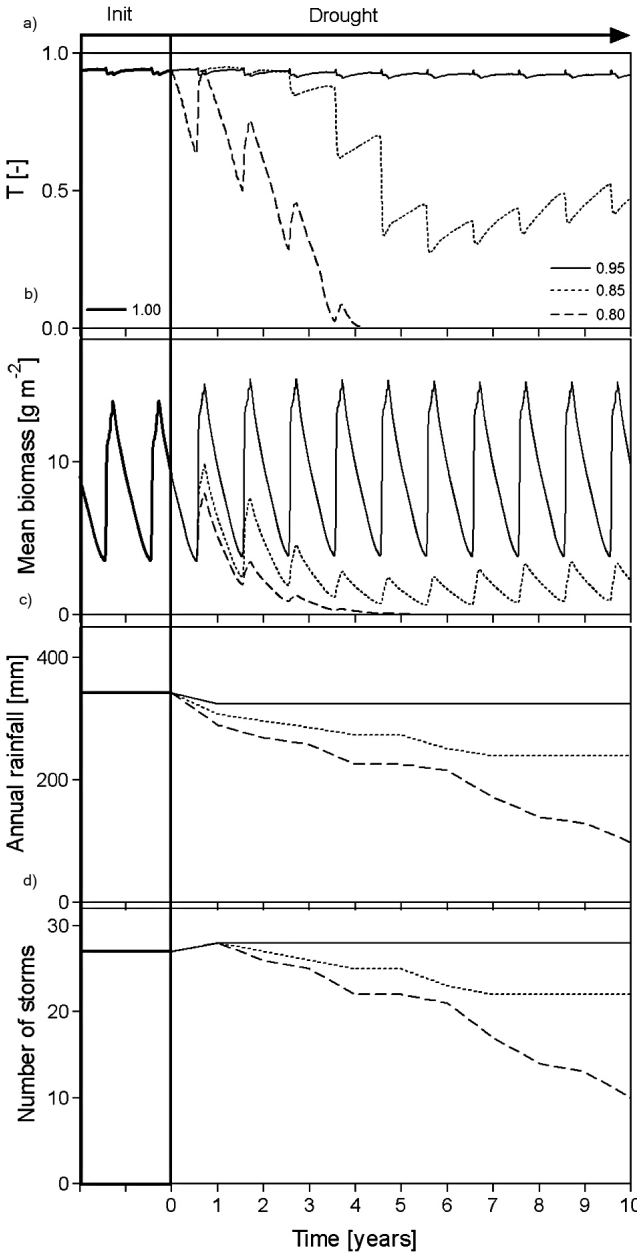

Figure 7. Evolution of the fully coupled system during drought for different reduced values of η_0, taken to be indicative of droughts of different magnitudes. (a) Biomass entropy I, middle), (b) mean biomass (g m^{-2}), (c) annual average rainfall (mm), and (d) number of storms per event. For each scenario, $\eta = \eta_{sc}\eta_{steady}$. All scenarios start at the same steady state with η_{sc} = 1.

[1] Auxiliary materials are available in the HTML. doi:10.1029/2011JG001748.

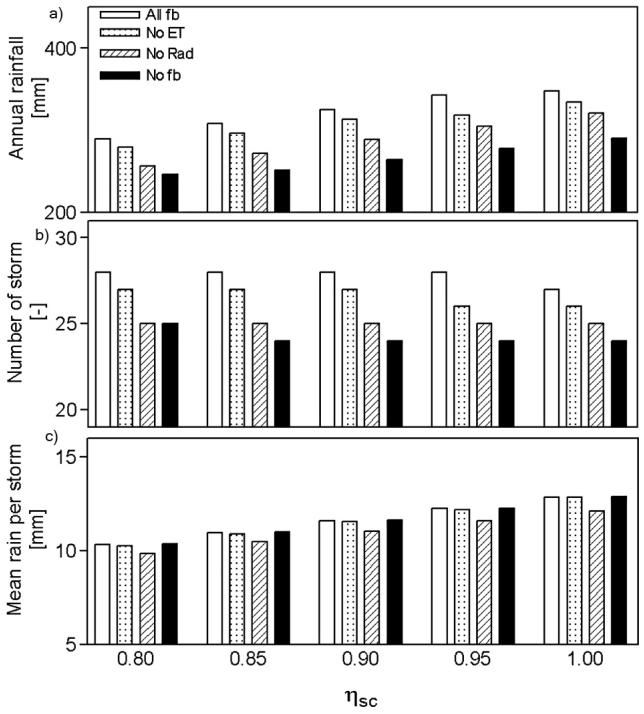

Figure 8. Rainfall statistics for the first year after the start of the drought simulation under different feedback scenarios. (a) Annual rainfall (mm), (b) number of individual storms, and (c) average rainfall depth per event (mm). The "all feedbacks" case consists of the fully coupled model as described in section 2. In the "no ET feedback case" and "no radiative feedback" case, the biomass influence on evapotranspiration and albedo, respectively, is removed when calculating fluxes to the atmosphere but not in calculating fluxes leaving the surface (that is, the fluxes are not physically consistent). In the "no feedbacks" case, the biomass influence on both evapotranspiration and albedo is removed.

cover becomes more sparse and patterns less pronounced (as reflected in the decrease in entropy). At the same time, rainfall decreases and the coupled system displays behavior that is qualitatively similar to that of the $\eta_{sc} = 0.80$ case. After the seventh year of the drought, rainfall stops decreasing. Although the precipitation driving the vegetation dynamics is now stationary, the vegetation pattern continues to evolve for several more seasons. Moreover, the dynamics actually reverse; that is, after year 7, mean biomass and entropy both *increase* rather than continuing to decrease. This occurs due to spatial redistribution of vegetation within a cluster, changing the amount of supported biomass over time. In this case, mean wet season biomass continues to change by more than 5% for the first 8 years of drought, while mean wet season entropy continues to change by more than 5% for the first 10 years of drought.

4.2. How Do the Two Types of Vegetation-Precipitation Feedbacks Affect the Response?

[37] The change of mean annual rainfall over the duration of each of the droughts indicates vegetation-precipitation feedbacks can significantly impact rainfall. For the $\eta_{sc} = 0.80$ case shown in Figure 7, the rainfall in the fourth year after the initiation of the drought is 63 mm/yr lower than during the first year of the drought, even though free atmospheric forcing parameters are identical in both years. This change is attributed to a decrease in the number of rainfall events occurring from 28 storms in year 1 to 22 storms in year 4 (Figure 7d). Land surface conditions change the anomaly size of the precipitation from 17% of its long-term average value in year 1 to 35% of the long-term average in year 4. Note that the feedback represented by this simulation includes both the direct effects of changes in vegetation cover and transpiration on precipitation and the effect of changes in soil moisture and ET on precipitation. The influence of the latter can be noted from the fact that rainfall for the $\eta_{sc} = 0.80$ case continues to decrease significantly after biomass has died out. This is due to a few days with atmospheric conditions such that rainfall occurrence is very sensitive to exact soil moisture values. Due to the fluctuations of the free atmospheric parameters used here, these events happen to occur relatively early in the season. Given the dry and highly seasonal precipitation regime of southwestern Niger, the presence or absence of individual rainfall events can significantly affect further land surface and precipitation evolution.

[38] When $\eta_{sc} = 0.95$, one would expect that a decrease in rainfall reduces biomass. However, biomass is actually increased relative to the steady state ($\eta_{sc} = 1$) case. Although rainfall decreases in the $\eta_{sc} = 0.95$ case, the difference in rainfall between the $\eta_{sc} = 1$ and $\eta_{sc} = 0.95$ cases is comparatively much smaller than the 5% decrease in η would suggest. The reduction in average rainfall per storm due to the decrease in the precipitation efficiency η is mitigated by the fact that a negative vegetation-precipitation feedback actually increases the number of storms in the $\eta_{sc} = 0.95$ case. A lower vegetation cover initiates a rainfall event more than halfway through the season. This storm has a larger effect on the biomass than the reduction in precipitation intensity (due to the reduction in η) during all storms, causing the overall mean biomass to be higher for $\eta_{sc} = 0.95$ than for $\eta_{sc} = 1.00$. However, the overall sign of the feedback indicates that in southwestern Niger, climate is such that the potential vegetation-precipitation feedbacks are positive more often than they are negative. This can be seen by the fact that annual rainfall decreases as vegetation decreases over the course of each of the droughts. Note that the increase in biomass when $\eta_{sc} = 0.95$ is not necessarily predictive of likely (or probable) observations. It serves merely to illustrate how exact feedback dynamics as determined by the evolution of atmospheric conditions may cause counter-intuitive changes in vegetation pattern morphology to occur.

[39] The seasonally averaged sign of the precipitation feedback can be "tested" for all values of η by explicitly removing feedbacks using the method described in section 3 and Figure 4. Figure 8 summarizes the effects of the vegetation-precipitation feedback on mean annual rainfall, number of storms per year, and average storm depth as a function of η_{sc}. These values change over the course of a given drought (as seen in Figure 7c), but only the average values for the first year of the drought are shown for the sake of simplicity. The mean annual rainfall value (Figure 7c) summarizes the average sign of each of the two feedback types (Figure 8a). The decrease in rainfall in the "no radiative feedback case" relative to the "all feedbacks case" implies that the radiative feedback promotes rainfall for higher

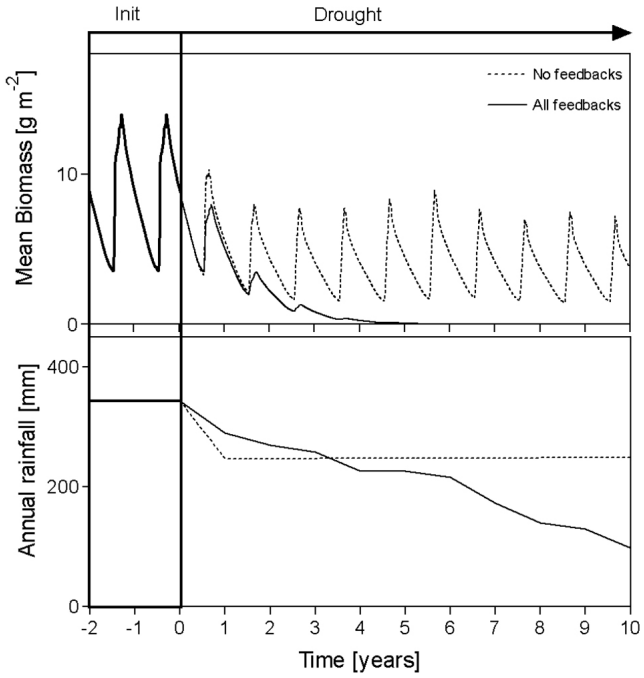

Figure 9. Evolution of coupled system after the initiation of drought at time 0 under "all feedbacks" and "no feedbacks" scenarios for η_{sc} = 0.80. (top) Mean biomass. (bottom) Annual rainfall. The two feedback scenarios are simulated as in Figure 8.

values of biomass, indicating a positive feedback between biomass and precipitation. The radiative feedback is consistently positive: since the state of the biomass during the wet season in the all-feedback case is higher than the constant biomass mask value used in the no-feedback case (by design), the surface albedo is lower in the all-feedback case, net radiation is higher, and surface fluxes are larger. The increased sensible heat flux causes the boundary layer to grow higher and faster, while the increased latent heat flux increases the specific humidity of the boundary layer, decreasing the lifting condensation level. This decrease in the LCL makes the initiation of a convective event more likely. The average depth per storm is essentially unaffected by the feedback presence, as shown by the "no radiative feedback" line in Figure 8c.

[40] On a seasonal scale, rainfall is also higher in the "all feedbacks case" than in the "no ET feedback case" with an artificially low constant biomass mask. Therefore, the evapotranspiration feedback is positive for all values of η. Because the effective biomass is higher in the presence of the evapotranspiration feedback, evapotranspiration is higher and the resulting atmospheric humidity and LCL height are lower, making the initiation of a convective rainfall event more likely.

[41] The size of the ET feedback is smaller than the size of the radiative feedback given the compensatory effects of increased soil evaporation and reduced transpiration (and biomass). Transpiration increases with biomass. However, the subsequent reduction in available soil moisture and the increase in shading cause bare soil evaporation to decrease, buffering the effect of a change in biomass on total evapotranspiration. Further compensation occurs between vegetated and bare areas through the redistribution of water. Due to the lateral re-distribution of water both above and below the surface, less water is available for bare soil evaporation from bare patches when transpiration from a vegetated cluster is increased. On average, rainfall amounts differ by more than 20% between the "all feedback" and "no feedbacks" cases, indicating vegetation-precipitation feedbacks are a key source of rainfall even in marginal drylands with low biomass amounts of patterned vegetation.

[42] Removing either only the radiative feedback or only the ET feedback barely changes the average rainfall depth per event, but removing both at the same time does cause a significant decrease. This implies that the effect of either of the feedbacks is amplified in the presence of the other one. This is not surprising, given that both feedbacks act by changing the atmospheric boundary layer.

[43] Figure 9 illustrates the effect of feedbacks on the response of vegetation patterns to drought. For simplicity, only a single value of η_{sc} is shown, $\eta\$_{sc}$ = 0.80, and only the "no feedbacks" and "all feedbacks" cases are shown. The feedbacks speed up desertification so much that they cause the vegetation to die off altogether where it might otherwise survive. Note also that in years one through three, the rainfall is higher in the "all feedbacks case" than in "no feedbacks" case, but the biomass is lower. This occurs because the net radiation is higher when feedbacks are present and the biomass can lower the albedo. This high net radiation causes the ABL to grow higher and to entrain much drier air, increasing the VPD. As a result of the increased atmospheric demand for vapor, the evapotranspiration increases significantly and the water available for biomass growth decreases. This causes the biomass to be lower even when rainfall is higher. This chain of causes illustrates the important of feedbacks between the vegetation and the ABL as well as feedbacks between the vegetation and rainfall. Furthermore, it shows that the effects of feedbacks change depending on atmospheric as well as surface conditions. This suggests that, to understand land surface dynamics over relatively short timescales, the effect of feedback cannot be parameterized and must be studied in reference to specific atmospheric conditions and biomass history.

5. Discussion and Conclusions

[44] Field observation of the timescales of vegetation pattern response to changes in rainfall are as of yet sparse and would require at least several decades of observation. Furthermore, observations may be difficult to interpret due to variability in rainfall. In the meantime, model results may provide estimates of the inertia of vegetation pattern morphology. In this paper, we have shown land-atmosphere feedbacks significantly affect this inertia. The feedbacks operate primarily through changing the radiative balance of the surface and therefore the heating of the boundary layer, but to a lesser extent also through changes in evapotranspiration. Therefore, at least in the Sahel, models of vegetation patterns that include vegetation-precipitation feedbacks are necessary before any quantitative inference on desertification tipping points can be made purely from spatial vegetation patterns and mean annual rainfall.

[45] This study addresses two specific questions: (1) How and how fast do modeled vegetation patterns respond to changes in rainfall regime? (2) How do vegetation-

precipitation feedbacks, both those acting through changes in the radiative balance and those acting through changes in evapotranspiration, affect this response? To answer question 1, the timescale of vegetation response to shifts in rainfall regime depends on the size of the change in rainfall. This timescale is generally on the order of at least 4–5 years for relatively large shifts in rainfall. This is likely to be less than the duration of a drought. In West Africa, for example, a 20-year wet period was followed by a 20-year dry period in the second half of the 20th century [*Le Barbé et al.*, 2002]. The adaptation timescale of 4–5 years can also be interpreted as the minimum length needed for field measurements that might study pattern adaptation to drought. In certain cases (in this study, in the $\eta_{sc} = 0.85$ case), vegetation adaptations to drought are not monotonic. That is, both mean biomass and pattern entropy change from decreasing to increasing at a certain point in the drought. This "overshooting" effect implies that there is a limit to the degree of specificity with which individual images of pattern morphology can be interpreted as indicators of desertification. An increase in pattern entropy and biomass is not necessarily indicative of an increase in the available water resources. Without site-specific parameters or knowledge of site-specific rainfall history, it is impossible to know how the system will respond to different future rainfall scenarios. Put differently, the system exhibits hysteresis not only at the desertification threshold (i.e., zero biomass), but also when patterned vegetation is present due to transient effects.

[46] To answer question 2 about the effect of vegetation-precipitation feedbacks, on a seasonally averaged level, both the radiative and the evapotranspiration feedback pathways are positive and cause a significant fraction of seasonal rainfall. The effect of local feedbacks on rainfall mainly occurs through changes in the number of storms, rather than in the duration of the wet season or in the average depth. Thus, a decrease in vegetation cover is exacerbated by a decrease in rainfall that causes further reductions in vegetation cover. This feedback not only increases the system sensitivity to interannual rainfall variability, but also speeds up the changes in pattern morphology associated with droughts. Note that the model used here is arguably more "coupled" than reality due to the assumption of a constant value of η for each scenario. In reality, stochastic elements cause fluctuations in η that might act to counter some of the initial dry/low vegetation perturbations that are propagated by the precipitation feedbacks. Hence, the timescale of 4–5 years estimated in this study must be viewed as a lower bound of the adaptation timescale. This may explain why the change timescale modeled here is faster than the timescale of the field study by *Barbier et al.* [2006], in which vegetation morphology measurements taken 40 years apart evolved from homogeneous cover to a spotted pattern (note also that the magnitude of drought in that study was lower than the ones modeled here).

[47] The evapotranspiration feedback has a smaller effect on the total rainfall than the radiative feedback, as compensation processes occur in space (between evaporation from bare soil patches and transpiration from vegetated patches) and time (between different days of the wet season) to limit the potential range of the total evapotranspiration contributing to rainfall. The bucket model used here to represent soil moisture may not capture all the water-based compensation effects. Transpiration is likely to access soil moisture from deeper layers than bare soil evaporation, decreasing the size of local-scale compensation. The root zone of vegetated areas are likely to extend beyond the areas with aboveground coverage [*Dunkerley*, 2000; *Gilad et al.*, 2007; *Barbier et al.*, 2008], amplifying the effect of compensation due to lateral re-distribution. The fact that vegetation influences rainfall primarily through influencing albedo is largely consistent with the conceptual model results of *Brovkin et al.* [1998]. It is also consistent with the conceptual model results of *Zheng and Eltahir* [1998], in which rainfall only responded to soil moisture anomalies when the surface radiation budget was allowed to respond to soil moisture. The difference between the sizes of the two feedbacks is particularly strong in cases with marginal biomass. In these cases, biomass has a large effect on albedo due to the cover change, but only a small effect on evapotranspiration because transpiration fluxes are small in comparison to soil evaporation fluxes.

[48] As indicated by the seasonally averaged sign, the sign of the vegetation cover-precipitation feedback is most often positive. However, depending on free atmospheric conditions, individual storms may be associated with a negative vegetation-precipitation feedback (i.e., rainfall only occurs when vegetation cover is low) [*Findell and Eltahir*, 2003; *Konings et al.*, 2010]. *van Heerwaarden et al.* [2010] also found a negative feedback between evapotranspiration and the atmospheric system in a case study of a single wet season day in Niamey, Niger. The variability in feedback sign can have a significant influence on the system response to drought if those individual events with a negative feedback causes large storms and subsequent increases in vegetation, as occurred when biomass increased under the reduction of rainfall in case $\eta_{sc} = 0.85$, and as occurred in the scenario depicted in Figure 9. This possibility suggests that the system can be very sensitive to the detailed conditions of individual scenarios, which might affect system evolution over several years. To be able to account for such strong sensitivity, stochastic models should be used to inform management decisions of patterned vegetation systems and to study the use of pattern morphology as indicators of ecosystem closeness to desertification.

[49] Feedbacks have a bigger effect on rainfall and cause a larger increase in the supported biomass when η, and average biomass, is relatively high. To preserve ecosystems close to desertification, irrigation measures may therefore be more useful for gapped systems or at the beginning of a drought than for spotted systems. Making such management decisions requires some expectation of how the drought evolves. Because the system may be sensitive to the exact land surface conditions under certain atmospheric conditions, small fluctuations in η driven by essentially stochastic factors (such as the availability of aerosols) and interannual variability in atmospheric forcings can cause large changes in expected system evolution, and differing implications for ecosystem management.

[50] Model imperfections may affect the predictions of this study, particularly the drought adaptation timescale of 4–5 years. As discussed above, the omission of stochastic forcing in the model causes this timescale to be a lower bound. Additional model imperfections exist that may cause this estimate to be too low. Because ecological measure-

ments for patterned vegetation systems in the Sahel are not very abundant, not all vegetation pattern parameters are known from field observations and many of the vegetation cover model parameters do not represent empirically grounded values (see Table 2). Furthermore, any minimalist model such as that used here necessarily ignores some processes. For example, cloud cover may occur on certain days even when rain does not. Such cloud cover decreases the incoming shortwave radiation (as well as the outgoing longwave radiation), decreasing the available net radiation at the surface and thus decreasing the surface sensible and latent heat fluxes. This may affect the rate of vegetation growth in a variety of ways: through reducing atmospheric temperatures and therefore respiration rates, or through affecting the atmospheric VPD, causing changes in the stomatal conductance and in the uptake rate of CO_2. Because vegetation growth is only integrated on a daily, rather than a sub-daily scale, such processes may not have a large effect on the model's performance at the annual level. Even if the model predictions made in this study are imperfect, they provide a first estimate of drought adaptation timescales in the presence of vegetation-precipitation feedbacks in the absence of long-term field measurements.

Appendix A

[51] The astronomical equation used for the incoming shortwave radiation is given by

$$R_s(t) = \frac{W_0}{r^2}\cos\beta, \tag{A1}$$

where $W_0 = 1353$ W m^{-2} is the solar constant, β is the zenith angle, and r is a correction factor for the Earth's distance from the sun as a function of the day of year DOY:

$$r = 1.0 + 0.017\cos\frac{2\pi}{365}(186 - \mathrm{DOY}) \tag{A2}$$

$$\cos\beta = \cos\varphi\cos h_a\cos\delta + \sin\phi\sin\delta, \tag{A3}$$

where h_a is the hour angle (i.e., fractional time of day expressed as an angle) and δ is the solar declension. φ is the latitude, here 15°.

[52] **Acknowledgments.** This paper grew out of discussions at the 2010 summer school on Biogeodynamics and Earth System Science at the Istituto Veneto di Scienze, Lettere, ed Arti. A. G. Konings was supported by the National Science Foundation (NSF) through the Graduate Research Fellowship Program. Dekker was supported by the high potential project from Utrecht University. Katul acknowledges support from the NSF (NSF-AGS-1102227, NSF-EAR-10-13339, and NSF-CBET-103347). Helpful comments from Sari Palmroth on the manuscript are gratefully acknowledged.

References

Avissar, R., and T. Schmidt (1997), An evalutation of the scale at which ground-surface heat flux patchiness affects the convective boundary layer using a large-eddy simulation model, *J. Atmos. Sci.*, *55*, 2666–2689.

Barbier, N., P. Couteron, J. Lejoly, V. Deblauwe, and O. Lejeune (2006), Self-organized vegetation patterning as a fingerprint of climate and human impact on semi-arid ecosystems, *J. Ecol.*, *94*(3), 537–547, doi:10.1111/j.1365-2745.2006.01126.x.

Barbier, N., P. Couteron, R. Lefever, V. Deblauwe, and O. Lejeune (2008), Spatial decoupling of facilitation and competition at the origin of gapped vegetation patterns, *Ecology*, *89*, 1521–1531.

Baudena, M., and A. Provenzale (2008), Rainfall intermittency and vegetation feedbacks in drylands, *Hydrol. Earth Syst. Sci.*, *12*, 679–689.

Baudena, M., F. D'Andrea, and A. Provenzale (2008), A model for soil-vegetation-atmosphere interactions in water-limited ecosystems, *Water Resour. Res.*, *44*, W12429, doi:10.1029/2008WR007172.

Brovkin, V., M. Claussen, V. Petoukhov, and A. Ganopolski (1998), On the stability of the atmosphere-vegetation system in the Sahara/Sahel region, *J. Geophys. Res.*, *103*(D24), 31,613–31,624.

Brutsaert, W. (1975), On a derivable formula for long wave radiation from clear skies, *Water Resour. Res.*, *11*, 743–744.

Brutsaert, W. (2005), *Hydrology: An Introduction*, Cambridge Univ. Press, 605 pp., Cambridge, U. K.

Charney, J. G. (1975), Dynamics of deserts and drought in the Sahel, *Q. J. R. Meteorol. Soc.*, *101*, 193–202.

Deblauwe, V., N. Barbier, P. Couteron, O. Lejeune, and J. Bogaert (2008), The global biogeography of semi-arid periodic vegetation patterns, *Global Ecol. Biogeogr.*, *17*(6), 715–723, doi:10.1111/j.1466-8238.2008.00413.x.

Deblauwe, V., P. Couteron,O. Lejeune, J. Bogaert, and N. Barbier (2011), Environmental modulation of self-organized periodic vegetation patterns in Sudan, *Ecography*, doi:/10.1111/j.1600-0587.2010.06694.x, in press.

de Boer, H. J., E. I. Lammertsma, F. Wagner-Cremer, D. L. Dilcher, M. J. Wassen, and S. C. Dekker (2011), Climate forcing due to optimization of maximal leaf conductance in subtropical vegetation under rising CO_2, *Proc. Natl. Acad. Sci. U.S.A.*, *108*, 4041–4046.

Dekker, S. C., M. Rietkerk, and M. F. P. Bierkens (2007), Coupling microscale vegetation-soil water and macroscale vegetation-precipitation feedbacks in semiarid ecosystems, *Global Change Biol.*, *13*(3), 671–678, doi:10.1111/j.1365-2486.2007.01327.x.

Dekker, S. C., H. J. de Boer, V. Brovkin, K. Fraedrich, M. J. Wassen, and M. Rietkerk (2010), Biogeophysical feedbacks trigger shifts in the modelled vegetation-atmosphere system at multiple scales, *Biogeosciences*, *7*, 1237–1245.

Dunkerley, D. (2000), Hydrologic effects of dryland shrubs: defining the spatial extent of modified soil water uptake rates at an Australian desert site, *J. Arid Environ.*, *45*, 159–172.

Ek, M. B., and A. A. M. Holtslag (2004), Influence of soil moisture on boundary layer cloud development, *J. Hydrometeorol.*, *5*(1), 86–99.

Findell, K. L., and E. A. B. Eltahir (2003), Atmospheric controls on soil moisture-boundary layer interactions. Part I: Framework development, *J. Hydrometeorol.*, *4*(3), 552–569.

Garratt, J. R. (1992), *The Atmospheric Boundary Layer*, 316 pp., Cambridge Univ. Press, Cambridge, U. K.

Gilad, E., J. von Hardenberg, A. Provenzale, M. Schachak, and E. Meron (2007), A mathematical model of plants as ecosystem engineers, *J. Theor. Biol.*, *244*, 680–691.

Grist, J. P., and S. E. Nicholson (2001), A study of the dynamic factors influencing the rainfall variability in the West African Sahel, *J. Clim.*, *14*, 1337–1359.

Guttal, V., and C. Jayaprakash (2007), Self-organization and productivity in semi-arid ecosystems: Implications of seasonality in rainfall, *J. Theor. Biol.*, *248*(3), 490–500, doi:10.1016/j.jtbi.2007.05.020.

Hermann, S. M., A. Anyamba, and C. J. Tucker (2005), Recent trends in vegetation dynamics of the African Sahel and their relationship to climate, *Global Environ. Change*, *15*, 394–404, doi:10.1016/j.gloenvcha.2005.08.004.

HilleRisLambers, R., M. Rietkerk, F. van den Bosch, H. H. T. Prins, and H. de Kroon (2001), Vegetation pattern formation in semi-arid grazing systems, *Ecology*, *82*(1), 50–61.

Janssen, R. H. H., M. B. J. Meinders, E. H. van Nes, and M. Scheffer (2008), Microscale vegetation-soil feedback boosts hysteresis in a regional vegetation-climate system, *Global Change Biol.*, *14*(5), 1104–1112, doi:10.1111/j.1365-2486.2008.01540.x.

Kader, B. A., and A. M. Yaglom (1990), Mean fields and fluctuation moments in unstably stratified turbulent boundary-layers, *J. Fluid Mech.*, *212*, 637–662.

Katul, G. G., D. S. Ellsworth, and C.-T. Lai (2000), Modeling assimilation and intercellular CO_2 from measured conductance: A synthesis of approaches, *Plant Cell Environ.*, *23*, 1313–1328.

Katul, G. G., S. Palmroth, and R. Oren (2009), Leaf stomatal responses to vapour pressure deficit under current and CO_2-enriched atmosphere explained by the economics of gas exchange, *Plant Cell Environ.*, *32*, 968–979.

Kefi, S., M. Rietkerk, and G. G. Katul (2008), Vegetation pattern shift as a result of rising atmospheric co2 in arid ecosystems, *Theor. Popul. Biol.*, *74*, 332–344.

Kim, C. P., and D. Entekhabi (1998), Feedbacks in the land-surface and mixed layer energy budgets, *Boundary Layer Meteorol.*, *88*, 1–21.

Kletter, A. Y., J. von Hardenberg, E. Meron, and A. Provenzale (2009), Patterned vegetation and rainfall intermittency, *J. Theor. Biol.*, *256*(4), 574–583, doi:10.1016/j.jtbi.2008.10.020.

Konings, A. G., G. G. Katul, and A. Porporato (2010), The rainfall-no rainfall transition in a coupled land-convective atmosphere system, *Geophys. Res. Lett.*, *37*, L14401, doi:10.1029/2010GL043967.

Koster, R. D., et al. (2004), Regions of strong coupling between soil moisture and precipitation, *Science*, *305*(5687), 1138–1140.

Koster, R. D., et al. (2006), GLACE: The Global Land-Atmosphere Coupling Experiment. Part I: Overview, *J. Hydrometeorol.*, *7*(4), 590–610.

Larcher, W. (2003), *Physiological Plant Ecology: Ecophysiology and Stress Physiology of Functional Groups*, 513 pp., Springer-Verlag, Berlin.

Le Barbé, L., T. Lebel, and D. Tapsoba (2002), Rainfall variability in West Africa during the years 1950–1990, *J. Clim.*, *15*, 187–202.

Lebel, T., J. D. Taupin, and N. D. Amato (1997), Rainfall monitoring during HAPEX-Sahel. 1. general rainfall conditions and climatology, *J. Hydrol.*, *188–189*, 74–96.

Nicholson, S. E., and P. J. Webster (2007), A physical basis for the interannual variability of rainfall in the sahel, *Q. J. R. Meteorol. Soc.*, *133*, 2065–2084, doi:10.1002/qj.104.

Ollson, L., L. Eklundh, and J. Ardö (2005), A recent greening of the Sahel—Trends, patterns and potential causes, *J. Arid Environ.*, *63*, 556–566, doi:10.1016/j.jaridenv.2005.03.008.

Oren, R., J. S. Sperry, G. G. Katul, D. E. Pataki, B. E. Ewers, N. Phillips, and K. V. R. Schafer (1999), Survey and synthesis of intra- and interspecific variation in stomatal sensitivity to vapour pressure deficit, *Plant Cell Environ.*, *22*(12), 1515–1526.

Ravi, S., P. D'Odorico, and G. Okin (2007), Hydrologic and aeolian controls on vegetation patterns in arid landscapes, *Geophys. Res. Lett.*, *34*, L24S23, doi:10.1029/2007GL031023.

Ravi, S., D. Breshaers, T. Huxman, and P. D'Odorico (2010), Land degradation in drylands: Interactions among hydrologic-aeolian erosion and vegetation dynamics, *Geomorphology*, *116*, 236–245, doi:10.1016/j.geomorph.2009.11.023.

Rietkerk, M., M. C. Boerlijst, F. van Langevelde, R. HilleRisLambers, J. van de Koppel, L. Kumar, H. H. T. Prins, and A. M. de Roos (2002), Self-organization of vegetation in arid ecosystems, *Am. Nat.*, *160*(4), 524–530.

Rietkerk, M., S. C. Dekker, P. C. de Ruiter, and J. van de Koppel (2004), Self-organized patchiness and catastrophic shifts in ecosystems, *Science*, *305*(5692), 1926–1929.

Saco, P., G. Willgoose, and G. Hancock (2007), Eco-geomorphology of banded vegetation patterns in arid and semi-arid regions, *Hydrol. Earth Syst. Sci.*, *11*, 1717–1730.

Santanello, J. A., M. A. Friedl, and M. B. Ek (2007), Convective planetary boundary layer interactions with the land surface at diurnal time scales: Diagnostics and feedbacks, *J. Hydrometeorol.*, *8*, 1082–1097, doi:10.1175/jhm614.1.

Scheffer, M., M. Holmgren, V. Brovkin, and M. Claussen (2005), Synergy between small- and large-scale feedbacks of vegetation on the water cycle, *Global Change Biol.*, *11*, 1003–1012.

Taylor, C. M., and R. J. Ellis (2006), Satellite detection of soil moisture impacts on convection at the mesoscale, *Geophys. Res. Lett.*, *33*, L03404, doi:10.1029/2005GL025252.

Thompson, S., G. Katul, and S. M. McMahon (2008), Role of biomass spread in vegetation pattern formation within arid ecosystems, *Water Resour. Res.*, *44*, W10421, doi:10.1029/2008WR006916.

Ursino, N., and S. Contarini (2006), Stability of banded vegetation patterns under seasonal rainfall and limited soil moisture storage capacity, *Adv. Water Resour.*, *29*(10), 1556–1564, doi:10.1016/j.advwatres.2005.11.006.

van de Koppel, J., et al. (2002), Spatial heterogeneity and irreversible vegetation change in semiarid grazing systems, *Am. Nat.*, *159*(2), 209–218.

van den Hurk, B., and E. van Meijgaard (2010), Diagnosing land-atmosphere interaction from a regional climate model simulation over West Africa, *J. Hydrometeorol.*, *11*(2), 467–481, doi:10.1175/2009jhm1173.1.

van Heerwaarden, C. C., J. V. G. de Arellano, A. F. Moene, and A. A. M. Holtslag (2009), Interactions between dry-air entrainment, surface evaporation and convective boundary-layer development, *Q. J. R. Meteorol. Soc.*, *135*(642), 1277–1291, doi:10.1002/qj.431.

van Heerwaarden, C. C., J. V. G. de Arellano, A. Gounou, F. Guichard, and F. Couvreux (2010), Understanding the daily cycle of evapotranspiration: A method to quantify the influence of forcings and feedbacks, *J. Hydrometeorol.*, *11*, 1405–1422, doi:10.1175/2010JHM1272.1.

Zheng, X., and E. Eltahir (1998), A soil moisture-rainfall feedback mechanism: 2. Numerical experiments, *Water Resour. Res.*, *34*, 777–785.

S. C. Dekker and M. Rietkerk, Department of Environmental Sciences, Copernicus Institute, Utrecht University, PO Box 80115, NL-3508 TC Utrecht, Netherlands.

G. G. Katul and A. G. Konings, Nicholas School of the Environment, Duke University, Box 90328, Durham, NC 27701, USA. (agk5@duke.edu)